









Study of a magnetically driven reconnection platform using ultrafast proton radiography

Cite as: Phys. Plasmas **26**, 062113 (2019); <https://doi.org/10.1063/1.5095960>

Submitted: 13 March 2019 . Accepted: 20 May 2019 . Published Online: 13 June 2019

Abraham Chien , Lan Gao , Hantao Ji , Xiaoxia Yuan , Eric G. Blackman , Hui Chen, Philip C. Efthimion, Gennady Fiksel , Dustin H. Froula , Kenneth W. Hill, Kai Huang , Quanming Lu, John D. Moody, and Philip M. Nilson



View Online



Export Citation



CrossMark



ULVAC

Leading the World with Vacuum Technology

- Vacuum Pumps
- Arc Plasma Deposition
- RGAs
- Leak Detectors
- Thermal Analysis
- Ellipsometers

Study of a magnetically driven reconnection platform using ultrafast proton radiography

Cite as: Phys. Plasmas **26**, 062113 (2019); doi: [10.1063/1.5095960](https://doi.org/10.1063/1.5095960)

Submitted: 13 March 2019 · Accepted: 20 May 2019 ·

Published Online: 13 June 2019



View Online



Export Citation



CrossMark

Abraham Chien,^{1,a)} Lan Gao,¹ Hantao Ji,¹ Xiaoxia Yuan,² Eric G. Blackman,³ Hui Chen,⁴ Philip C. Efthimion,¹ Gennady Fiksel,⁵ Dustin H. Froula,⁶ Kenneth W. Hill,¹ Kai Huang,⁷ Quanming Lu,⁷ John D. Moody,⁴ and Philip M. Nilson⁶

AFFILIATIONS

¹Princeton Plasma Physics Laboratory, Princeton University, Princeton, New Jersey 08543, USA

²Department of Astronomy, Beijing Normal University, Beijing 100875, China

³Department of Physics and Astronomy, University of Rochester, Rochester, New York 14627, USA

⁴Lawrence Livermore National Laboratory, Livermore, California 94550, USA

⁵Department of Nuclear Engineering and Radiological Sciences, University of Michigan, Ann Arbor, Michigan 48109, USA

⁶Laboratory for Laser Energetics, University of Rochester, Rochester, New York 14623, USA

⁷CAS Key Laboratory of Geospace Environment, Department of Geophysics and Planetary Science, University of Science and Technology of China, Hefei 230026, China

^{a)}Electronic mail: achien2@pppl.gov

ABSTRACT

A novel magnetically driven reconnection platform was created by a pair of U-shaped Cu coils that connect two parallel Cu plates irradiated at a focused laser intensity of $\sim 3 \times 10^{16}$ W/cm² and characterized using ultrafast proton radiography. The proton data show two prolate voids, each corresponding to the coil current, with an inferred maximum magnitude of 57 ± 4 kA. A center “flasklike” feature was also observed in the proton radiographs. By prescribing electromagnetic fields associated with magnetic reconnection in proton ray tracing simulations, characteristics of this center feature were reproduced. These results demonstrate the robustness of the laser-driven capacitor coils for generating strong magnetic fields and provide promise of using such coils as a viable platform for studying magnetically driven reconnection in the laboratory.

Published under license by AIP Publishing. <https://doi.org/10.1063/1.5095960>

I. INTRODUCTION

Magnetic reconnection is a ubiquitous plasma phenomenon characterized by the breaking and reconnecting of magnetic field lines,¹ with wide-ranging applications to low- β plasmas such as coronal mass ejections^{2,3} and solar flares.^{4,5} Among the outstanding questions in magnetic reconnection is the nonthermal particle acceleration. There is ample observational evidence of a nonthermal particle spectrum^{6–8} attributed to reconnection. While several theories describing acceleration mechanisms exist,^{9–11} they are untested in laboratory plasmas. Dedicated laboratory reconnection experiments, such as MRX (Magnetic Reconnection Experiment)¹² and VTF (Versatile Toroidal Facility),¹³ utilize low- β plasmas to produce magnetically driven, axisymmetric reconnection. Significant experimental results have been generated for quantitative comparisons with theory and numerical simulations in studies of the classic Sweet–Parker MHD model,^{14,15} two-fluid effects,^{16–18} the electron diffusion region,^{19,20} and energy partitioning,²¹ to name a few. Direct detection of the

nonthermal charged particles, however, has been limited due to short Debye lengths for local *in situ* measurements and short mean free paths for remote measurements.

In recent years, magnetic reconnection experiments in laser-driven high-energy-density (HED) plasmas have been intensively investigated. These experiments either build on the self-generated magnetic fields by the Biermann battery mechanism,^{22–26} where intense lasers irradiate a foil target, or apply a compact external magnetic field generator on two colliding plasma plumes.²⁷ While remote detection of nonthermal charged particles becomes feasible for these hot HED plasmas, the reconnection process is strongly driven by plasma flows, a situation less relevant to most space and astrophysical applications.

A robust platform for generating strong external magnetic fields has emerged more recently using intense lasers and a unique capacitor-coil target. First introduced by Korobkin²⁸ in 1979, the technique has been developed by many groups^{29–38} and provides a reliable method to generate up to kiloTesla magnetic fields.^{39,40} Such capacitor

coil targets are generally composed of two parallel metallic plates (the capacitor) connected with thin wires in different geometric shapes. Hot electrons are generated as the laser beam hits the back plate,^{41,42} which builds up a voltage difference between the front and back plates and drives a large current through the connecting coil. This large current therefore results in strong magnetic field generation.

In this paper, we develop a magnetically driven, quasisymmetric reconnection platform using laser-driven capacitor coils with more direct relevance to space and astrophysical plasmas and an ultimate goal of studying particle acceleration. The target design is based on two parallel U-shaped Cu coils connecting two Cu plates. The voltage built between the two capacitor plates drives currents through both coils, forming a quasisymmetric magnetic reconnection geometry between the coils. This reconnection geometry is similar to that from MRX and, thus, termed “micro-MRX”. Similar targets made out of Ni were previously studied using an optical probe.³⁵ By contrast, in our study, ultrafast proton radiography of the reconnection geometry was performed to characterize the platform. The proton data show two prolate voids due to proton deflections by the currents in the coils, from which $\sim 31\text{--}44\text{ kA}$ currents in each coil at $\sim 3\text{--}6\text{ ns}$ after laser irradiation were inferred. In the reconnection region between the two coils, a center “flasklike” feature has also been observed in the proton radiographs. By prescribing electromagnetic fields from in-plane electrical fields and out-of-plane currents in the proton ray tracing simulations, this center feature is recovered and consistent with magnetic reconnection processes.

The paper is organized as follows. Section II describes the experimental setup. Section III presents the experimental results and interpolation of the experimental observations using proton ray tracing calculations. Section IV provides discussions of our analyses. Section V summarizes the results and future work based on this study, in particular, particle acceleration due to magnetic reconnection.

II. EXPERIMENTAL SETUP

The experiments were conducted on the OMEGA EP Laser System at the Laboratory of Laser Energetics, University of Rochester. Two EP long pulse beams [total energy 2.5 kJ, square pulse duration

1 ns, 351 nm wavelength (3ω)] were used to drive the main interaction. A maximum intensity of $\sim 3 \times 10^{16}\text{ W/cm}^2$ on target is achieved. A schematic of the target chamber geometry is shown in Fig. 1(a).

The targets are made of two parallel Cu plates (square, $1500\text{ }\mu\text{m}$ length, $50\text{ }\mu\text{m}$ thickness) connected by two parallel U-shaped Cu coils (square cross section, $50\text{ }\mu\text{m}$ thickness) separated by an intercoil distance of $600\text{ }\mu\text{m}$. The U-shaped coils are comprised of two parallel straight sections of $500\text{ }\mu\text{m}$ length connected with a semicircle with a radius of $300\text{ }\mu\text{m}$. Two laser entrance holes are formed in the front foil, allowing the long-pulse beams to pass through and focus onto the back foil. These lasers irradiate the rear plate, generating a beam of superthermal hot electrons. These hot electrons stream onto the front plate and build up an electrical potential between the plates. This results in large parallel currents flowing through the coils from the back plate toward the front plate, generating strong magnetic fields around the coils. In the intercoil region, an antiparallel field structure is formed. Due to the curvature of the coils, this results in a quasisymmetric 2-D reconnection geometry, with the normal to the reconnection plane aligned along the tangent of the coil curvature. A zoomed-in view of the main target coils is detailed in Fig. 1(b); the magnetic field structure and resulting reconnection plane are shown. The coil currents rise to a maximum until the laser pulses are turned off and then subsequently decay. The decay in current corresponds to a decrease in the driven magnetic field, driving pull reconnection.¹²

Electromagnetic fields were diagnosed with TNSA (target normal sheath acceleration)⁴³ proton radiography. Up to 60 MeV protons are generated⁴⁴ by irradiating a $20\text{ }\mu\text{m}$ -thick Cu foil with the 0.3 kJ, 1 ps OMEGA EP backlighter. The energetic protons stream $\sim 7\text{ mm}$ toward the main interaction target coil region. The Lorentz force from local electromagnetic fields deflects the protons, and they are finally deposited onto a radiochromic film (RCF) pack $\sim 80\text{ mm}$ from the coil region. The RCF pack is composed of alternating layers of Al filters and films, allowing measurement for various proton energies. The timing of the short-pulse backlighter relative to the main interaction lasers enables time-dependent analysis of the field structure.

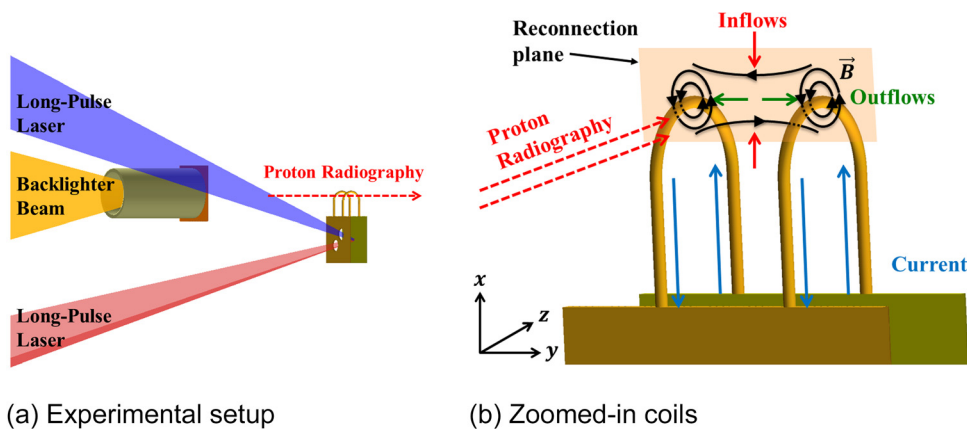


FIG. 1. (a) Experimental setup on OMEGA EP. As the EP long-pulse beams irradiate the back Cu plate and build a voltage between the two parallel plates, strong currents are generated in each of the coils creating antiparallel magnetic fields between the coils. (b) shows a zoomed-in view of the coils and coil currents, along with the reconnection field geometry. A sample reconnection plane is shown for the top-most wire segment. This reconnection plane can be swept, following the coil currents to form the quasisymmetric 2-D geometry. (a) Experimental setup. (b) Zoomed-in coils.

III. EXPERIMENTAL RESULTS

Proton radiographs were taken of the target region at $\sim 3, 4,$ and 6 ns after the start of the long-pulse laser beams. Taking into account time-of-flight for the energetic protons to reach the target area, the radiographs represent field measurements at $t = 3.158, 4.149,$ and 6.137 ns with respect to the beginning of the square pulse. The experimental radiograph for $t = 3.158$ ns is shown in the right panel of Fig. 2. The square copper foil and target stalk can be seen in the image, as well as the two coils as viewed from the target face-on direction. The primary feature is the formation of two prolate voids that are generated by the magnetic field from the driven coil currents. An additional center “flasklike” structure between the voids is also observed and is analyzed in more detail below.

For analysis of proton radiography images, synthetic radiographs are generated via a particle ray-tracing code. Local magnetic fields are calculated with the Biot-Savart law. To calculate the coil-generated magnetic field, the semicircular coil is discretized into 50 equal-length current-carrying segments. The magnetic field from the coils is computed for vertices in a cubic mesh (2.5 mm side length, $5 \mu\text{m}$ mesh size) centered around the coil region. Details on calculations of prescribed reconnection-motivated fields are described in Secs. III B 1 and III B 2. In the ray-tracing simulation, protons are advanced via a fourth-order adaptive Runge-Kutta algorithm. At each time step, the local electrical and magnetic fields are calculated at the proton location using trilinear interpolation from the electromagnetic field mesh. The mesh is shown to be sufficiently fine by comparing synthetic radiographs using precalculated mesh fields with those using closed-form magnetic field profiles for simple geometries, such as a circular current loop.

A. Prolate void due to driven coil current

The size of the prolate voids created by the U-shaped coils has been shown to scale as $r \propto I^{0.5} E_p^{-0.25}$, where r is the size of the void, I is the coil current, and E_p is the proton energy.³³ By comparing the size of the voids with synthetic radiographs, coil current can be

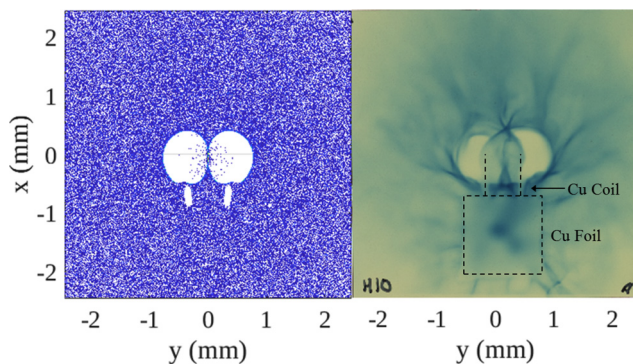


FIG. 2. Synthetic radiographs of coil-generated magnetic fields compared with experimental data. The left panel shows a synthetic radiograph of the “vacuum field” with a coil current of $I = 44$ kA, scaled to the target plane. A comparison with the experimental data (right panel) indicates close agreement in structure and size of the primary feature. Here, $t = 3.158$ ns, $E_p = 24.7$ MeV.

inferred for the three time measurements. A comparison of the synthetic image with experimental data for $t = 3.158$ ns is shown in Fig. 2.

Coil current was inferred for the three proton radiography measurements, and the time evolution is shown in Fig. 3. From the lumped-circuit model of capacitor-coil operation,³⁴ the current roughly undergoes exponential decay with time after the laser is turned off. The exponential fit implies a decay time constant of $\tau \sim 8.6 \pm 1.6$ ns. The current decay time can be approximated by an RL circuit with time constant L/R . Compared to a capacitor-coil target with 1 coil, the load resistance and inductance are both halved, resulting in a similar L/R value for the two cases. Resistance and inductance are approximated as $R \sim 0.1 \Omega$ and $L \sim 1.2$ nH, respectively,³⁴ giving an estimated $\tau \sim L/R = 12$ ns, consistent with the experimental measurement. Extrapolating the current magnitude to $t = 1$ ns, the maximum coil current is inferred to be $\sim 57 \pm 4$ kA, which corresponds to a coil center magnetic field strength of ~ 110 T. This measured coil current is significantly higher than that reported in Ref. 33 due to an improved target design avoiding current shorting in between the two Cu plates. Plasma parameters were not experimentally measured, so we assume an electron density $n_e = 10^{18} \text{ cm}^{-3}$ and temperature $T_e = 500$ eV based on experimental measurements on a similar configuration.⁴⁵ Thus, the plasma beta is ~ 0.02 , which is in the low-beta regime that we wish to experimentally replicate.

B. Center bubble feature related to magnetic reconnection

In addition to the primary feature, a center “flasklike” bubble with relatively high proton fluence between the two prolate voids is observed. This feature is not present in synthetic radiographs simulated with only the coil magnetic fields (Fig. 2). Motivated by a magnetic reconnection picture, two primary candidates that can potentially explain the center bubble structure are explored: an in-plane electric field E_{in} and an out-of-plane current density J_{out} . Both fields can generate the center feature by providing an opposing force to the deflecting coil magnetic fields, thus allowing an area of higher proton fluence between the voids.

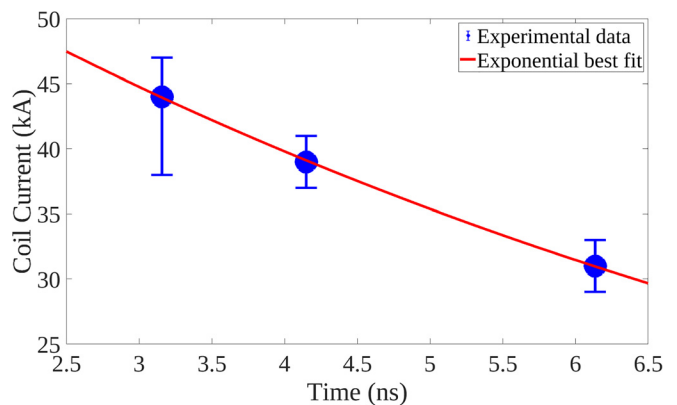


FIG. 3. Time evolution of coil current as measured by proton radiography at $t = 3.158, 4.149,$ and 6.137 ns. The data points are calculated from radiographs with proton energy $E_p = 24.7$ MeV. The red line indicates an exponential decay fit and is used to infer the coil current at $t = 1$ ns (at laser turn-off). The decreasing trend of the coil current over time implies a pull reconnection regime.

1. In-plane electric field

In fast magnetic reconnection, an in-plane electric field (hereafter referred to as E_{in}) is often generated. During pull reconnection, this electric field can be directed along the outflow direction [see Fig. 1(b)]. In a Cartesian coordinate system with $\pm y$ as the outflow direction, $\pm x$ as the inflow direction, and z out of plane, the in-plane electric field can be written as⁴⁶

$$E_y = v_{ez}B_x - \frac{1}{ne} \frac{\partial}{\partial x} p_{e,xy} - \frac{1}{ne} \frac{\partial}{\partial y} p_{e,yy} - \frac{1}{2e} \frac{\partial}{\partial y} m_e v_{e,y}^2. \quad (1)$$

Here, E is the electric field, v_e is the electron velocity, B is the magnetic field, n is the electron density, e is the electron charge, m_e is the electron mass, p_e is the electron pressure tensor, and the x , y , and z subscripts represent the corresponding directional components. The largest contribution to E_y has been shown in particle-in-cell simulations⁴⁶ to be $v_{ez}B_x$, with the remaining smaller terms with opposite signs, which reduces the magnitude of E_y . $v_{ez}B_x$ is, therefore, a good approximation for an upper bound on E_{in} . The direction of E_{in} is toward the outflow direction, namely, along $+y$ for $y > 0$ and along $-y$ for $y < 0$. An estimate of the expected electric field magnitude can then be calculated as $E_{in} \sim v_{ez}B_x \sim (j_{ez}/en_e)B_x$. We assume a current sheet aspect ratio of $\delta/L \sim 0.1$ (typical for fast reconnection⁴⁷), and in the incompressible, steady-state limit, the magnetic field ratio can be approximated as the aspect ratio, giving $B_y/B_x \sim L/\delta \sim 10$. We estimate the out-of-plane electron current as $j_{ez} \sim B_y/(\mu_0\delta_e)$, $E_{in} \sim 0.1B_y v_{A,e}$ where $v_{A,e} = B_y/\sqrt{\mu_0 n_e m_e}$ is the electron Alfvén velocity and δ_e is the electron skin depth. Plasma density was not experimentally measured, so in the calculation, an estimated value of $n_e \sim 10^{18} \text{ cm}^{-3}$ is assumed. Magnetic field strength is approximated as $B \sim 100 \text{ T}$. The resulting estimate of the in-plane electric field strength is $E_{in} \sim 9.3 \times 10^8 \text{ V/m}$.

To study the effect of such an electric field, synthetic radiographs were generated with the addition of an artificial electric field to model the in-plane field described above. Along every azimuthal slice of the semicircular coil, the electric field is calculated as a Gaussian distribution

$$E_{in} = E_0 \tanh(y/\delta_y) \exp(-y^2/\delta_y^2) \exp(-(x-a)^2/\delta_x^2), \quad (2)$$

where y is the outflow direction, x is the inflow direction, $a = 300 \mu\text{m}$ is the radius of the semicircle, and $\delta_y = \delta_x = 150 \mu\text{m}$ are the “widths” of the electric field distribution in the outflow and inflow directions, respectively. For simplicity, an aspect ratio of $\delta_y/\delta_x = 1$ is chosen. Since azimuthal symmetry is assumed, E_{in} has no dependence on the out-of-plane coordinate θ . Values of E_0 were tuned to best match the experimental data. As with the magnetic field calculation from the driven coil current, the prescribed electric field is calculated for points on the same mesh to enable faster ray-tracing computation.

Figure 4 shows the synthetic proton data with prescribed in-plane reconnection electric field compared to the experimental data. The “flasklike” structure is well-replicated in terms of the maximum width and general shape using $E_0 = 2.0 \times 10^{10} \text{ V/m}$. This required field magnitude is ~ 20 times larger than our estimation shown above.

2. Out-of-plane current

An out-of-plane current sheet is a frequent indicator of magnetic reconnection. The current is distributed over the current sheet, creating an out-of-plane current density (henceforth referred to as J_{out}). The direction of J_{out} depends on whether push or pull reconnection occurs: J_{out} is antiparallel to the driven coil current during push reconnection and parallel to the coil current during pull reconnection. As the proton radiography measurements are taken well past the laser turning off, and therefore, as current is decreasing (Fig. 3), pull reconnection is expected. In the analysis, J_{out} is, therefore, assumed to be parallel to the coil current.

An estimate can be made of the magnitude of the out-of-plane current. Assume a simple current sheet with thickness δ , $J_{out} \sim B/(\mu_0\delta)$. The total current can then be written as $I_{out} \sim J_{out}\delta L = BL/\mu_0$, where L is the length of the current sheet. Taking $L \sim 200 \mu\text{m}$ (one-third the intercoil distance), $I_{out} \sim 16 \text{ kA}$. A hard upper bound is established by the magnitude of the coil currents: since the current sheet forms as a response to the decrease in the coil currents, $I_{out} < 2I_{coil}$.

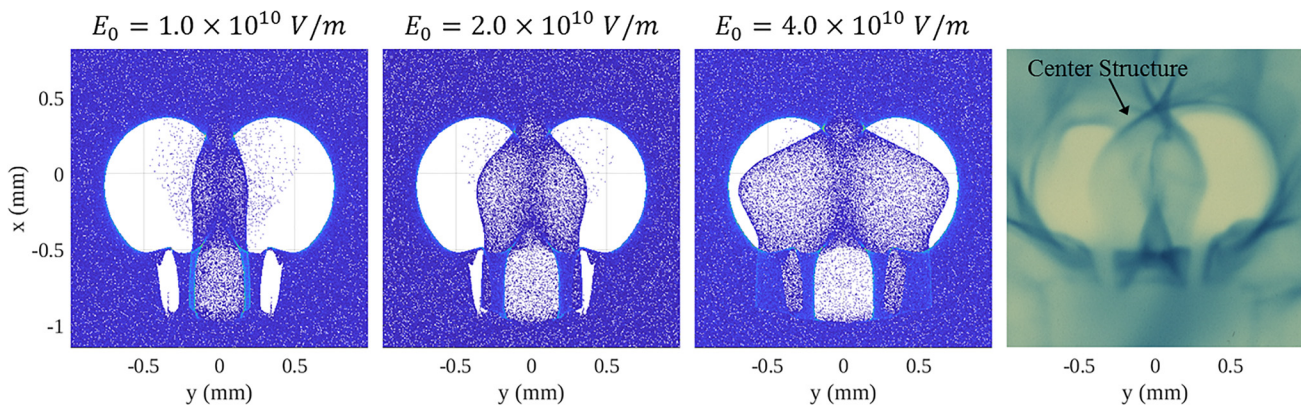


FIG. 4. Synthetic radiographs of E_{in} with different electric field magnitude E_0 for 24.7 MeV protons (from left to right: $E_0 = 1.0 \times 10^{10} \text{ V/m}$, $E_0 = 2.0 \times 10^{10} \text{ V/m}$, $E_0 = 4.0 \times 10^{10} \text{ V/m}$), compared with experimental data taken at $t = 3.158 \text{ ns}$ (rightmost panel). In the synthetic radiographs, the electric field profile is given by $E_{in} = E_0 \tanh(y/\delta_y) \exp(-y^2/\delta_y^2) \exp(-(x-a)^2/\delta_x^2)$, with $\delta_y = \delta_x = 150 \mu\text{m}$, giving an aspect ratio of 1. $I_{coil} = 44 \text{ kA}$ is taken from the inferred coil current from vacuum field comparisons. The center bubble structure increases in size as E_0 increases. An estimate of experimental E_0 can be determined by matching the maximum width of the center structures: this analysis implies $E_{0,exp} \sim 2.0 \times 10^{10} \text{ V/m}$. Also note the close match in shape between the $E_0 = 2.0 \times 10^{10} \text{ V/m}$ case and the experimental data.

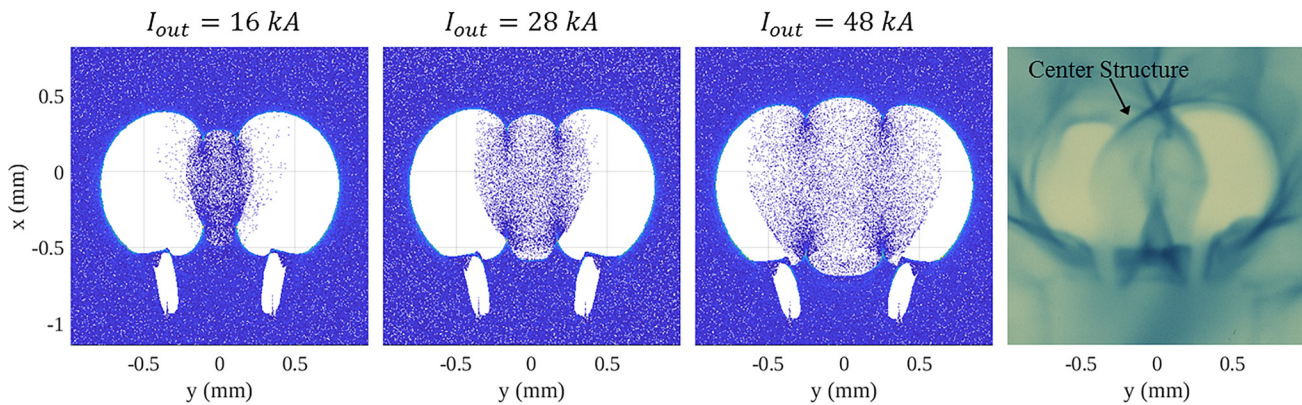


FIG. 5. Synthetic radiographs of J_{out} with different total out-of-plane current I_{out} for 24.7 MeV protons (from left to right: $I_{out} = 16$ kA, $I_{out} = 28$ kA, $I_{out} = 48$ kA), compared with experimental data taken at $t = 3.158$ ns (rightmost panel). In the synthetic radiographs, the current sheet is modeled as a rectangle with dimensions $100 \mu\text{m} \times 80 \mu\text{m}$ to maintain an aspect ratio ~ 1 , and $I_{coil} = 44$ kA. The center bubble structure increases in size as I_{out} increases. An estimate of experimental I_{out} can be determined by matching the maximum width of the center structures: this analysis implies $I_{out, exp} \sim 28$ kA.

The above current sheet approximation of I_{out} comfortably falls within this constraint.

For synthetic ray-tracing simulations, the current sheet can be approximated as a rectangular region centered between the coils. Due to the azimuthal symmetry, this 2-D current density profile is swept along θ to match the coil geometry. Dimensions are chosen as $L \times \delta = 100 \mu\text{m} \times 80 \mu\text{m}$ to maintain an aspect ratio close to unity. The artificial current distribution is simulated by multiple wires spaced evenly on a rectangular mesh with separation $10 \mu\text{m}$, with each wire carrying an equal fraction of the total current. The Biot-Savart law is again used to compute the resulting magnetic field from the current sheet: each wire is subdivided into 50 segments, and the magnetic field contributions are summed for each wire segment on grid vertices. Driven coil currents are taken to be $I_{coil} = 44$ kA, as inferred from Fig. 3. Figure 5 shows synthetic radiographs for different current magnitudes for the chosen current sheet. Qualitatively, it is observed that the center structure grows in size with increasing J_{out} .

A match to experiment is obtained by comparing synthetic radiographs with experimental data. The current magnitude is tuned to best match the maximum widths of the center feature. Using this method, the total out-of-plane current is inferred as $I_{out} \sim 28$ kA. Despite the matched width, the shape of the feature generated by the artificial field does not match the experimental feature well. This can be attributed to the many other parameters of the current sheet that are not well-understood: shape and dimensions of the current sheet, tilt of the current sheet, current distribution within the current sheet, and location of the current sheet relative to the coils. In addition, 3D reconnection effects that are not covered by the existing 2D model may be responsible for the observed differences. In our study, crude assumptions were made regarding these parameters, but further work is needed to better model the current sheet.

In addition, the inclusion of I_{out} changes the void feature caused by the driven coil current. This effect can be seen in Fig. 5, where the two prolate voids are clearly bigger in the $I_{out} = 48$ kA case, compared with the $I_{out} = 16$ kA case. Therefore, in our out-of-plane current model, the estimated value of the coil current shown in Fig. 3 overestimates the true coil current. This, in turn, overestimates the out-of-plane current, as the size of the center structure is determined

by force balance between the magnetic fields generated by the two currents. To obtain a best fit consistent with the model, both values of I_{out} and I_{coil} are tuned simultaneously. This best fit is given by $I_{coil} = 41$ kA and $I_{out} = 26$ kA (an overlay of the synthetic radiograph on experimental data is shown in Fig. 6). As expected, the best fit currents are smaller than the originally estimated values of $I_{coil} = 44$ kA and $I_{out} = 28$ kA. The error bar for the $t = 3.158$ ns data point in Fig. 3 is extended downward to account for the decrease in inferred I_{coil} .

A comparison of the artificial out-of-plane current magnitude with the earlier estimate of ~ 16 kA shows relatively good agreement. In addition, the current easily falls within the upper bound constraint.

IV. DISCUSSION

In Sec. III, reconnection-related E_{in} and J_{out} were investigated as possible candidates to explain the center “flasklike” bubble feature. With the information we currently have, it is difficult to identify the

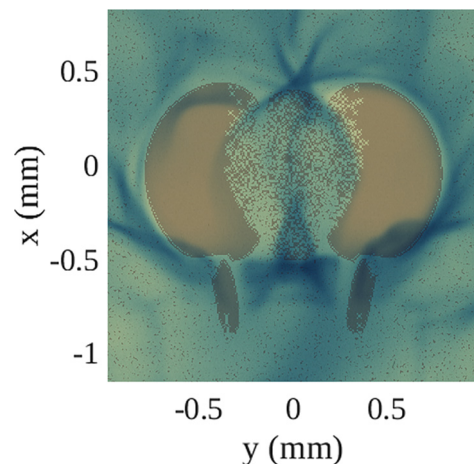


FIG. 6. An overlay of a synthetic radiograph with $I_{coil} = 41$ kA and $I_{out} = 26$ kA on experimental data. This represents a best fit of the out-of-plane current model with experiment, defined by matching the size of the prolate voids and the maximum width of the center feature.

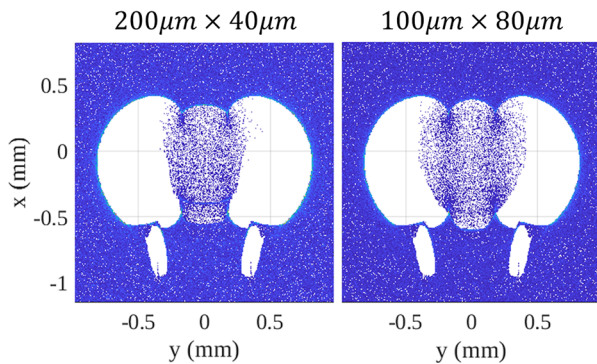


FIG. 7. Synthetic radiographs of J_{out} with the same total out-of-plane current $I_{out} = 30$ kA but different current sheet dimensions. In both cases, the current sheet is modeled as a rectangle with constant current density but with dimensions $200 \mu\text{m} \times 40 \mu\text{m}$ (left panel) and $100 \mu\text{m} \times 80 \mu\text{m}$ (right panel). $I_{coil} = 44$ kA and $E_p = 24.7$ MeV to match experiment. Despite the same current density magnitude, the resulting center structure shape and width are dramatically different. This indicates that further research is needed to determine the shape and structure of the current sheet as it plays a large role in understanding the proton radiography data and reconnection physics.

dominance of the two candidates in creating such feature. For example, a decrease in the plasma density can result in a higher E_{in} , making the estimated electric field more consistent with our ray tracing results. In the out-of-plane current case, the bubble size from J_{out} is dependent on current sheet dimensions. As is shown in Fig. 7, for the same out-of-plane current $I_{out} = 30$ kA, the bubble size for a $100 \mu\text{m} \times 80 \mu\text{m}$ current sheet is larger than that for a $200 \mu\text{m} \times 40 \mu\text{m}$ current sheet. The inferred I_{out} of 28 kA is based on dimensions of $100 \mu\text{m} \times 80 \mu\text{m}$ in our analysis, and that value can change depending on the actual current sheet size. Further experiments are being planned to evaluate the strength of the two candidates. Plasma parameters will be measured using interferometry or optical Thomson scattering. By probing the reconnection region in face-on (TNSA protons approaching the target from the front) and back-on (TNSA protons approaching the target from the back) directions for proton radiography, contributions from electric and magnetic fields can be distinguished because the proton deflection from electric fields remains the same for face-on and back-on radiography while magnetic field deflection orientations are opposite for the two cases.

In addition, the shape of the simulated center feature for J_{out} does not match the data very well. This can be attributed to the multitude of parameters that can be tuned in addition to current sheet size: the shape of the current sheet, the angle of the current sheet with respect to the coils, current distributions in the current sheet, the location of the current sheet, and 3D effects. More fluid and particle-in-cell simulations are being performed to get insights into these parameters.

V. CONCLUSIONS

In conclusion, MG-level antiparallel magnetic fields generated by a pair of U-shaped coil currents creating a magnetically driven reconnection geometry were directly measured by proton radiography. The measured coil current amplitude was ~ 44 kA, 39 kA, and 31 kA, at 3.158, 4.149, and 6.137 ns after laser irradiation, respectively. This corresponds to an estimated 57 ± 4 kA maximum current at the time of laser turn-off and a 110 T magnetic field at coil center. The measured

currents and magnetic fields were ~ 2 times larger than reported in our previous work³³ due to an improved target design involving the removal of a plastic spacer between the foils.

A center “flasklike” bubble feature was observed in the proton radiographs. The feature was compared to synthetic proton images with artificial fields motivated by magnetic reconnection: E_{in} and J_{out} . Both candidates seem to generate correct proton deflections. E_{in} is shown to reproduce the center bubble shape with a field strength ~ 20 times higher than our simple calculations. J_{out} is shown to provide good agreement with constraints and estimates on the current sheet strength. With an assumed rectangular current sheet ($100 \mu\text{m} \times 80 \mu\text{m}$), the maximum width of the center structure is matched with $I_{out} = 28$ kA. However, the shape of the feature is difficult to match due to several parameters of the current sheet that are not well-understood: in particular, the shape and positioning of the current sheet and current density distribution within can affect the feature significantly, and they are not accounted for in this study. It is demonstrated that the dimensions of the current sheet have a large impact on the shape and size of the resulting bubble feature. Further experiments need to be performed to measure plasma parameters as well as better understand current shape and positions to identify the dominant contributions.

The fact that characteristics of the center feature were recovered by prescribing electromagnetic fields associated with magnetic reconnection shows promise of using such coils as a viable platform for studying magnetically driven reconnection in the laboratory. Our next focus will be an intense study of particle acceleration using this platform and comparisons with space and astrophysical observations.

ACKNOWLEDGMENTS

This work was supported by the National Laser Users Facility Program by the National Nuclear Security Administration (NNSA) under Grant No. NA0003608. The authors express their gratitude to General Atomics and the Laboratory for Laser Energetics (LLE) for target fabrication, and to the OMEGA EP crew for technical support.

REFERENCES

- ¹M. Yamada, R. Kulsrud, and H. Ji, *Rev. Mod. Phys.* **82**, 603 (2010).
- ²S. Antiochos, C. DeVore, and J. Klimchuk, *Astrophys. J.* **510**, 485 (1999).
- ³P. Cassak, D. Mullan, and M. Shay, *Astrophys. J.* **676**, L69 (2008).
- ⁴E. Parker, *Astrophys. J. Suppl.* **8**, 177 (1963).
- ⁵K. Shibata and T. Magara, *Living Rev. Sol. Phys.* **8**, 6 (2011).
- ⁶S. Krucker, H. S. Hudson, L. Glesener, S. M. White, S. Masuda, J.-P. Wuelser, and R. P. Lin, *Astrophys. J.* **714**, 1108 (2010).
- ⁷M. Tavani, A. Bulgarelli, V. Vittorini, A. Pellizzoni, E. Striani, P. Caraveo, M. Weisskopf, A. Tennant, G. Pucella, and A. Trois, *Science* **331**, 736 (2011).
- ⁸A. Abdo, M. Ackermann, M. Ajello, A. Allafort, L. Baldini, J. Ballet, G. Barbiellini, D. Bastieri, K. Bechtol, and R. Bellazzini, *Science* **331**, 739 (2011).
- ⁹J. F. Drake, M. Swisdak, H. Che, and M. A. Shay, *Nature* **443**, 553 (2006).
- ¹⁰M. Oka, M. Fujimoto, I. Shinohara, and T. D. Phan, *J. Geophys. Res.* **115**, A08223, <https://doi.org/10.1029/2010JA015392> (2010).
- ¹¹M. Hoshino, *Phys. Rev. Lett.* **108**, 135003 (2012).
- ¹²M. Yamada, H. Ji, S. Hsu, T. Carter, R. Kulsrud, N. Bretz, F. Jobses, Y. Ono, and F. Perkins, *Phys. Plasmas* **4**, 1936 (1997).
- ¹³J. Egedal, A. Fasoli, M. Porkolab, and D. Tarkowski, *Rev. Sci. Instrum.* **71**, 3351 (2000).
- ¹⁴H. Ji, M. Yamada, S. Hsu, and R. Kulsrud, *Phys. Rev. Lett.* **80**, 3256 (1998).
- ¹⁵H. Ji, M. Yamada, S. Hsu, R. Kulsrud, T. Carter, and S. Zaharia, *Phys. Plasmas* **6**, 1743 (1999).

- ¹⁶J. Birn, J. Drake, M. Shay, B. Rogers, R. Denton, M. Hesse, M. Kuznetsova, Z. Ma, A. Bhattacharjee, A. Otto, and P. Pritchett, *J. Geophys. Res.* **106**, 3715, <https://doi.org/10.1029/1999JA900449> (2001).
- ¹⁷Y. Ren, M. Yamada, S. Gerhardt, H. Ji, R. Kulsrud, and A. Kuritsyn, *Phys. Rev. Lett.* **95**, 055003 (2005).
- ¹⁸M. Yamada, Y. Ren, H. Ji, J. Breslau, S. Gerhardt, R. Kulsrud, and A. Kuritsyn, *Phys. Plasmas* **13**, 052119 (2006).
- ¹⁹Y. Ren, M. Yamada, H. Ji, S. Gerhardt, and R. Kulsrud, *Phys. Rev. Lett.* **101**, 085003 (2008).
- ²⁰H. Ji, Y. Ren, M. Yamada, S. Dorfman, W. Daughton, and S. P. Gerhardt, *Geophys. Res. Lett.* **35**, L13106, <https://doi.org/10.1029/2008GL034538> (2008).
- ²¹M. Yamada, J. Yoo, J. Jara-Almonte, H. Ji, R. M. Kulsrud, and C. E. Myers, *Nat. Commun.* **5**, 4774 (2014).
- ²²P. M. Nilson, L. Willingale, M. C. Kaluza, C. Kamperidis, S. Minardi, M. S. Wei, P. Fernandes, M. Notley, S. Bandyopadhyay, M. Sherlock, R. J. Kingham, M. Tatarakis, Z. Najmudin, W. Rozmus, R. G. Evans, M. G. Haines, A. E. Dangor, and K. Krushelnick, *Phys. Rev. Lett.* **97**, 255001 (2006).
- ²³C. K. Li, F. H. Séguin, J. A. Frenje, J. R. Rygg, R. D. Petrasso, R. P. J. Town, P. A. Amendt, S. P. Hatchett, O. L. Landen, A. J. Mackinnon, P. K. Patel, M. Tabak, J. P. Knauer, T. C. Sangster, and V. A. Smalyuk, *Phys. Rev. Lett.* **99**, 015001 (2007).
- ²⁴L. Willingale, P. M. Nilson, M. C. Kaluza, A. E. Dangor, R. G. Evans, P. Fernandes, M. G. Haines, C. Kamperidis, R. J. Kingham, C. P. Ridgers, M. Sherlock, A. G. R. Thomas, M. S. Wei, Z. Najmudin, K. Krushelnick, S. Bandyopadhyay, M. Notley, S. Minardi, M. Tatarakis, and W. Rozmus, *Phys. Plasmas* **17**, 043104 (2010).
- ²⁵J. Zhong, Y. Li, X. Wang, J. Wang, Q. Dong, C. Xiao, S. Wang, X. Liu, L. Zhang, L. An, F. Wang, J. Zhu, Y. Gu, X. He, G. Zhao, and J. Zhang, *Nat. Phys.* **6**, 984 (2010).
- ²⁶A. E. Raymond, C. Dong, A. Mckelvey, C. Zulick, N. Alexander, A. Bhattacharjee, P. T. Campbell, H. Chen, V. Chvykov, E. Del Rio, P. Fitzsimmons, W. Fox, B. Hou, A. Maksimchuk, C. Mileham, J. Nees, P. M. Nilson, C. Stoeckl, A. Thomas, and L. Willingale, *Phys. Rev. E* **98**, 043207 (2018).
- ²⁷G. Fiksel, W. Fox, A. Bhattacharjee, D. H. Barnak, P. Y. Chang, K. Germaschewski, S. X. Hu, and P. M. Nilson, *Phys. Rev. Lett.* **113**, 105003 (2014).
- ²⁸V. Korobkin and S. L. Motylev, *Sov. Tech. Phys. Lett.* **5**, 474 (1979).
- ²⁹J. F. Seely, *Appl. Phys. B* **31**, 37 (1983).
- ³⁰H. Daido, F. Miki, K. Mima, M. Fujita, K. Sawai, H. Fujita, Y. Kitagawa, S. Nakai, and C. Yamanaka, *Phys. Rev. Lett.* **56**, 846 (1986).
- ³¹S. Fujioka, Z. Zhang, K. Ishihara, K. Shigemori, Y. Hironaka, T. Johzaki, A. Sunahara, N. Yamamoto, H. Nakashima, T. Watanabe, H. Shiraga, H. Nishimura, and H. Azechi, *Sci. Rep.* **3**, 1170 (2013).
- ³²C. Courtois, A. D. Ash, D. M. Chambers, R. A. D. Grundy, and N. C. Woolsey, *J. Appl. Phys.* **98**, 054913 (2005).
- ³³L. Gao, H. Ji, G. Fiksel, W. Fox, M. Evans, and N. Alfonso, *Phys. Plasmas* **23**, 043106 (2016).
- ³⁴G. Fiksel, W. Fox, L. Gao, and H. Ji, *Appl. Phys. Lett.* **109**, 134103 (2016).
- ³⁵X. X. Pei, J. Y. Zhong, Y. Sakawa, Z. Zhang, K. Zhang, H. G. Wei, Y. T. Li, Y. F. Li, B. J. Zhu, T. Sano, Y. Hara, S. Kondo, S. Fujioka, G. Y. Liang, F. L. Wang, and G. Zhao, *Phys. Plasmas* **23**, 032125 (2016).
- ³⁶C. Goyon, B. B. Pollock, D. P. Turnbull, A. Hazi, L. Divol, W. A. Farmer, D. Haberberger, J. Javedani, A. J. Johnson, A. Kemp, M. C. Levy, B. Grant Logan, D. A. Mariscal, O. L. Landen, S. Patankar, J. S. Ross, A. M. Rubenchik, G. F. Swadling, G. J. Williams, S. Fujioka, K. F. F. Law, and J. D. Moody, *Phys. Rev. E* **95**, 033208 (2017).
- ³⁷V. T. Tikhonchuk, M. Bailly-Grandvaux, J. J. Santos, and A. Poyé, *Phys. Rev. E* **96**, 023202 (2017).
- ³⁸X. Yuan, J. Zhong, Z. Zhang, W. Zhou, J. Teng, Y. Li, B. Han, D. Yuan, J. Lin, C. Liu, Y. Li, B. Zhu, H. Wei, G. Liang, W. Hong, S. He, S. Yang, Y. Zhao, Z. Deng, F. Lu, Z. Zhang, B. Zhu, K. Zhou, J. Su, Z. Zhao, Y. Gu, G. Zhao, and J. Zhang, *Plasma Phys. Controlled Fusion* **60**, 065009 (2018).
- ³⁹J. J. Santos, M. Bailly-Grandvaux, L. Giuffrida, P. Forestier-Colleoni, S. Fujioka, Z. Zhang, P. Korneev, R. Bouillaud, S. Dorard, D. Batani, M. Chevrot, J. E. Cross, R. Crowston, J.-L. Dubois, J. Gazave, G. Gregori, E. dHumires, S. Hulin, K. Ishihara, S. Kojima, E. Loyez, J.-R. Marques, A. Morace, P. Nicola, O. Peyrusse, A. Poy, D. Raffestin, J. Ribolzi, M. Roth, G. Schaumann, F. Serres, V. T. Tikhonchuk, P. Vacar, and N. Woolsey, *New J. Phys.* **17**, 083051 (2015).
- ⁴⁰K. F. F. Law, M. Bailly-Grandvaux, A. Morace, S. Sakata, K. Matsuo, S. Kojima, S. Lee, X. Vaisseau, Y. Arikawa, A. Yogo, K. Kondo, Z. Zhang, C. Bellei, J. J. Santos, S. Fujioka, and H. Azechi, *Appl. Phys. Lett.* **108**, 091104 (2016).
- ⁴¹D. W. Forslund, J. M. Kindel, and K. Lee, *Phys. Rev. Lett.* **39**, 284 (1977).
- ⁴²J. S. Pearlman and G. H. Dahlbacka, *Appl. Phys. Lett.* **31**, 414 (1977).
- ⁴³S. C. Wilks, A. B. Langdon, T. E. Cowan, M. Roth, M. Singh, S. Hatchett, M. H. Key, D. Pennington, A. MacKinnon, and R. A. Snavely, *Phys. Plasmas* **8**, 542 (2001).
- ⁴⁴L. Gao, P. M. Nilson, I. V. Igumenshchev, M. G. Haines, D. H. Froula, R. Betti, and D. D. Meyerhofer, *Phys. Rev. Lett.* **114**, 215003 (2015).
- ⁴⁵D. Haberberger, S. Ivancic, S. X. Hu, R. Boni, M. Barczys, R. S. Craxton, and D. H. Froula, *Phys. Plasmas* **21**, 056304 (2014).
- ⁴⁶J. F. Drake, M. A. Shay, and M. Swisdak, *Phys. Plasmas* **15**, 042306 (2008).
- ⁴⁷Y.-H. Liu, M. Hesse, F. Guo, W. Daughton, H. Li, P. A. Cassak, and M. A. Shay, *Phys. Rev. Lett.* **118**, 085101 (2017).